Hindawi Publishing Corporation
Journal of Nanomaterials
Volume 2015, Article ID 201650, 8 pages
http://dx.doi.org/10.1155/2015/201650

Research Article

Synthesis and Characterization of Hierarchical Structured TiO_2 Nanotubes and Their Photocatalytic Performance on Methyl Orange

Kai Liu,[1] Shiwei Lin,[1,2] Jianjun Liao,[2] Nengqian Pan,[1] and Min Zeng[1]

[1]*Key Laboratory of Ministry of Education for Advanced Materials in Tropical Island Resources, College of Materials and Chemical Engineering, Hainan University, Haikou 570228, China*
[2]*College of Information Science & Technology, Hainan University, Haikou 570228, China*

Correspondence should be addressed to Shiwei Lin; linsw@hainu.edu.cn

Received 5 December 2014; Revised 16 February 2015; Accepted 7 March 2015

Academic Editor: Amir Kajbafvala

Hierarchical structured TiO_2 nanotubes were prepared by mechanical ball milling of highly ordered TiO_2 nanotube arrays grown by electrochemical anodization of titanium foil. Scanning electron microscopy, transmission electron microscopy, X-ray diffraction, specific surface area analysis, UV-visible absorption spectroscopy, photocurrent measurement, photoluminescence spectra, electrochemical impedance spectra, and photocatalytic degradation test were applied to characterize the nanocomposites. Surface area increased as the milling time extended. After 5 h ball milling, TiO_2 hierarchical nanotubes exhibited a corn-like shape and exhibited enhanced photoelectrochemical activity in comparison to commercial P25. The superior photocatalytic activity is suggested to be due to the combined advantages of high surface area of nanoparticles and rapid electron transfer as well as collection of the nanotubes in the hierarchical structure. The hierarchical structured TiO_2 nanotubes could be applied into flexible applications on solar cells, sensors, and other photoelectrochemical devices.

1. Introduction

Compared with photocatalysis (PC), photoelectrocatalysis (PEC) is more efficient and effective. In PEC system, a photoanode is used as the working electrode, instead of directly dispersing catalyst into the wastewater. What is more, during the degradation process of the pollutants in the water, PEC could also generate hydrogen at a low bias voltage under the irradiation of solar light [1, 2].

For PEC, the fundamental requirement for high solar energy conversion is that the material should have good photoelectrochemical response ability as well as high stability. Among the plentiful semiconductor catalysts, TiO_2 photocatalysts are one type of attractive and promising materials due to their excellent properties such as high photocatalytic activity, stability, nontoxicity, and low price [3]. Recently, highly ordered TiO_2 nanotube arrays (TNTAs) have been fabricated using a simple electrochemical anodization process and demonstrated to be with potential applications such as gas sensors [4], solar cells [5], photodegradation [6], and water splitting [7]. TiO_2 nanotube arrays possess large internal surface area, direct electron transfer path, and low recombination rate [8–11], enabling us to achieve a higher photocatalytic activity and efficiency. However, due to the rigidity in the planar structure, the electrode connections for sensors or solar cells are difficult and thus pose a challenge in practical use. Therefore, the porous nanostructured TiO_2 film in the form of particles is still desirable in practical applications. The present ways to prepare hierarchical structure materials are using hydrothermal method with previously mechanical mixing [12, 13] or subsequently deposition [2], which are not efficient and homogenous.

In this work, we reported the fabrication of hierarchical structured anatase TiO_2 nanotubes in gram-scale via a facile two-step approach: highly ordered uniform TiO_2 nanotube arrays were first grown by conventional electrochemical anodization of titanium foil, followed by mechanical ball milling. The geometrical structure could be easily controlled

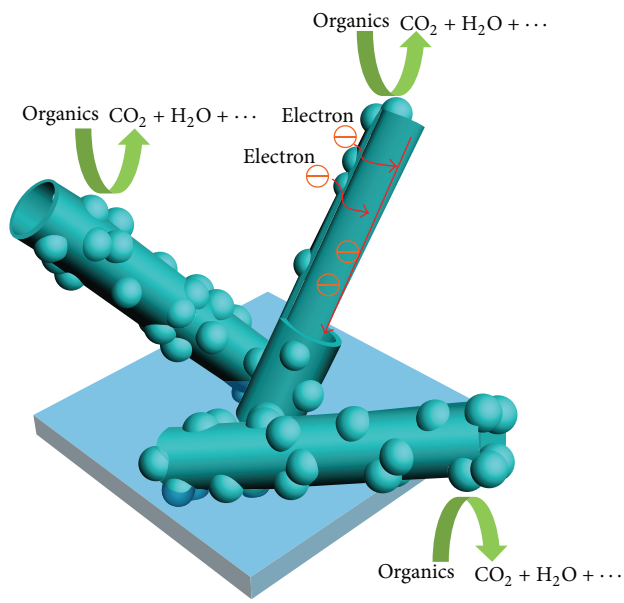

Scheme 1: Illustration of the large surface area and efficient charge carrier collection as well as transfer in the hierarchical structured TiO_2 nanotubes.

by milling duration. Further, the photocatalytic efficiency varies with the milling time. The preferable photocatalytic activity can be attributed to the combined advantages of high surface area of nanoparticles and efficient charge carrier collection as well as fast electron transfer of the nanotubes in the hierarchical structure (as shown in Scheme 1). Besides the application in the formaldehyde detector in our previous report [14], hierarchical structured TiO_2 nanotubes by this two-step method show superior photoelectrochemical properties.

2. Experimental Section

2.1. Fabrication of Hierarchical Structured TiO_2 Nanotubes. Anodization method was used to prepare TNTAs. A large piece of raw titanium foil with thickness of 0.5 mm was cut into small pieces of $40 \times 50\,mm^2$, which were then cleaned with acetone, ethanol, and deionized water for 15 min, successively. Anodization was performed in a two-electrode configuration with Ti foil as the working electrode and stainless steel foil as the counter electrode. The interspace between the working and counter electrodes was about 3 cm. A direct current power supply was used as the voltage source to drive the anodization. The electrolyte consisted of 0.3 wt% NH_4F and 2 vol% H_2O in ethylene glycol. Ti foil was anodized at 60 V for 24 h at room temperature. After anodization, nanotubes were removed from Ti foil by sonication in water for 5 min. To achieve crystalline structure, nanotubes were annealed at 500°C for 3 h in air with a heating rate of 2°C/min.

1.0 g as-prepared TiO_2 nanotubes were weighed out and placed in a laboratory plastic ball mill, together with 0.5 mL ethanol and 10.0 g agate balls (5.0 mm in diameter) as milling media. The grinding was conducted in a shaker mill (QM-3B, Nanjing NanDa Instrument Plant) that was operated at the speed of 600 rpm for 0.5, 5, and 10 h, respectively. The dispersant was 0.2 mL glycerol which was added in the last 5 min of the milling process.

2.2. Electrophoretic Deposition of Hierarchical Structured TiO_2 Film. The hierarchical structured TiO_2 nanotubes were suspended in 2-propanol to a concentration of 1 mg/mL under 1 h sonication. Electrophoretic deposition (EPD) method was applied to fabricate TiO_2 films onto fluorine-doped tin oxide (FTO) glass at 100 V/cm.

2.3. Sample Characterization. Field-emission scanning electron microscope (FESEM) images were obtained at 15 kV accelerating voltage (Hitachi S4800). Close examination of the hierarchical structure was further carried out by transmission electron microscopy (TEM, JEOL 2100). X-ray diffraction (XRD) was performed on a diffractometer (Bruker D8) using CuK_α as the radiation source. XRD patterns were collected between 2θ of 20–80° at a scan rate of 2° per min. Specific surface area determined by Brunauer-Emmett-Teller (BET) method was investigated by specific surface area and pore size analyzer (Beckman Coulter SA3100). UV-visible absorption measurement of TiO_2 films was carried on UV-visible spectroscopy (Persee TU-1901). Photoluminescence (PL) spectra were recorded via a photoluminescence spectrometer (Hitachi F-7000) with an excitation wavelength of 300 nm at room temperature.

2.4. Electrochemical Measurements. Photocurrents of the as-prepared TiO_2 films were analyzed by electrochemical workstation (Zanher Zennium) in a three-electrode system with a platinum foil counter electrode (1 cm × 1 cm) and a saturated calomel reference electrode. The working electrode was illuminated with UV light (370 nm, $100\,mW/cm^2$). The electrolyte was 1 M sodium sulfate aqueous solution. Electrochemical impedance spectra (EIS) were carried out by

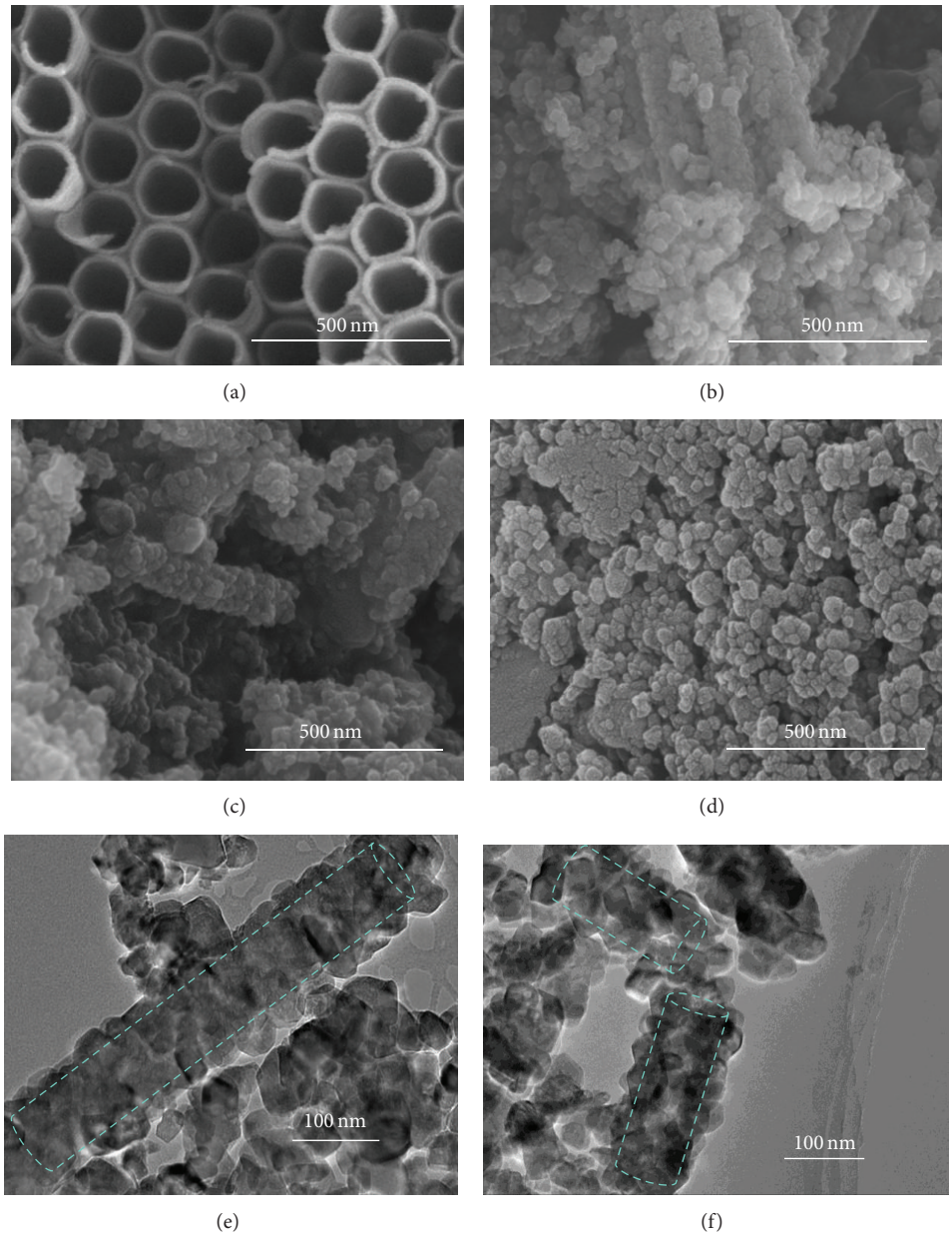

Figure 1: FESEM images of as-prepared TiO_2 nanotube arrays (a) and hierarchical structured TiO_2 fabricated after different ball milling time: (b) 0.5 h, (c) 5 h, and (d) 10 h. TEM investigation of 0.5 h (e) and 5 h (f) milled samples.

applying bias of the open-circuit voltage under 100 mW·cm^{-2} illumination and were recorded over a frequency range from 1 kHz to 0.01 Hz with ac amplitude voltage of 10 mV.

2.5. Photocatalytic and Photoelectrochemical Degradation of Methyl Orange. Photocatalytic activities and photoelectrochemical catalytic activities of TiO_2 films were measured by examining the degradation behavior of methyl orange (MO). Before experiments started, MO solution with photoanode was kept in the dark for 30 min to achieve adsorption/desorption equilibrium. Then the photoelectrodes were irradiated by a 300 W high-pressure mercury lamp with strongest wavelength of 365 nm (Bilon GGZ300). The interval between the lamp and the electrode surface was 5 cm. Photoelectrochemical catalytic measurements were performed with an additional DC power supply to provide 1.0 bias voltage. The initial concentration of MO solution was 5 mg/L. The pH value of MO solution was adjusted to 2 using 1 M H_2SO_4. For photoelectrochemical catalysis, sodium sulfate was added to the acidic MO solution reaching the concentration of 0.2 M. The MO degradation during catalytic reaction was monitored by UV-visible spectrophotometer.

3. Results and Discussion

3.1. Morphology of Hierarchical Structured TiO_2 Nanotubes. Figures 1(a)–1(d) show FESEM images of TiO_2 nanotube

arrays and samples under different milling time. All images were taken under the same magnification and microscope settings. Figure 1(a) indicates that nanotubes were uniformly formed and loosely connected to each other. The contact between nanotubes is weak and breakable, which allows the formation of dispersed nanotubes. Of the nanotubes, the diameter is about 110 nm and the wall-thickness is in a range from 10 to 20 nm. Figures 1(b) and 1(c) indicate that nanotube arrays were broken into discrete nanotubes and crushed into fragments during the mechanical milling process. After being milled for 0.5 h, some of the nanotubes turned into small pieces and adhered to the outer walls of other nanotubes. When the milling time was extended to 5 h, the surface morphology appeared to be uniform, and nanotubes were completely dispersed into individual ones and coated with nanoparticles homogeneously. The hierarchical structured nanotubes exhibit corn-like shape. Nanotubes were ground into nanoparticles totally after 10 h of milling, and nanoparticles heavily aggregated as shown in Figure 1(d).

TEM investigation was shown in Figures 1(e) and 1(f). TEM images show the close examination of hierarchical structured TiO_2 nanotubes. After 20 min of ultrasonic treatment to prepare the TEM sample, nanoparticles still adhere to nanotubes uniformly, indicating that the bonding force between nanoparticles and nanotubes is strong. The close contact provides a direct way for nanotubes to collect charge carriers from nanoparticles.

3.2. Crystalline Phases of Hierarchical Structured TiO_2 Nanotubes and P25. Figure 2 shows XRD patterns of the hierarchical TiO_2 nanotubes and P25. It was found that the nanotubes prepared by anodization without annealing were amorphous (black line). The annealing process performed at 500°C in atmosphere could generate a uniform structure of anatase phase (red line). Furthermore, XRD patterns gave no obvious indication of rutile phase. That is to say, no phase change occurred in the annealed samples during the ball milling process [15, 16]. Commercial P25 has both anatase and rutile phase. And the mass fraction of rutile (X_R) and anatase (X_A) of P25 was determined using the following equation [17]:

$$X_R = \frac{1}{1 + 1.26\left(I_A/I_R\right)} \times 100\%, \quad (1)$$

where I_A and I_R are the intensities of anatase (101) and rutile (110) peaks, respectively. The content of anatase and rutile in P25 is 86.25% and 13.75%, respectively.

3.3. Specific Surface Areas of Hierarchical TiO_2 Nanotubes. Specific surface areas data are shown in Figure 3. As milling time prolonged, specific surface area increased. Specific surface areas of detached nanotube arrays are 27.87 m^2/g and become 32.47 m^2/g, 42.14 m^2/g, and 42.70 m^2/g after 0.5 h, 5 h, and 10 h of milling, respectively. After 0.5 h, 5 h, and 10 h of milling, the values of specific surface area increased by 16.5%, 51.2%, and 53.2% compared to pristine nanotubes, which is due to the rising proportion of nanoparticles.

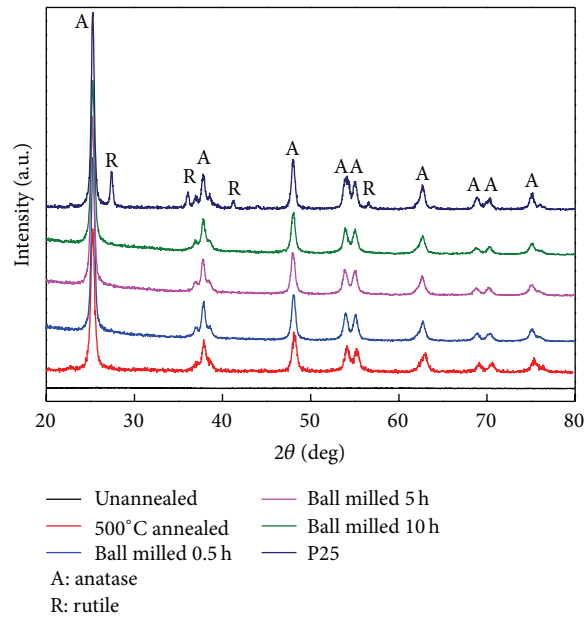

Figure 2: X-ray diffraction patterns of different TiO_2 samples.

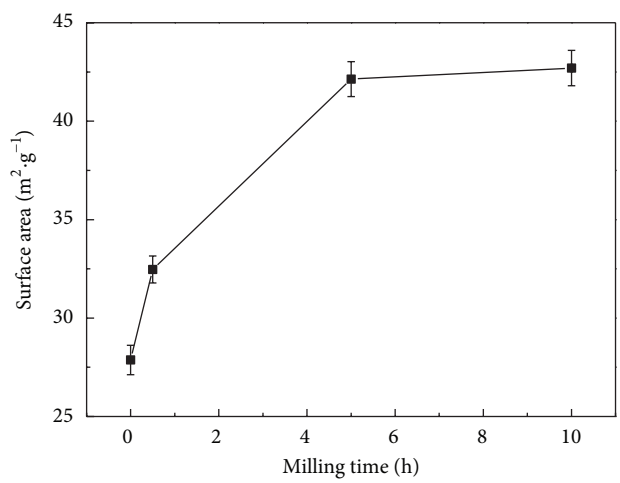

Figure 3: Specific surface areas of TiO_2 nanotubes after different milling time (with error bars).

3.4. UV-Visible Absorption Spectra of TiO_2 Films. Light absorption of TiO_2 films was measured by UV-visible spectroscopy as shown in Figure 4. P25 (black line) and manually ground TiO_2 nanotubes (red line) had higher absorption than ball milled TNTAs. The manually ground sample mostly consisted of nanotubes because of the relatively mild comminution. Nanotubes could increase light scattering; thus an enhanced light absorption was observed [12]. Commercial P25 contains rutile phase, which could absorb more light than anatase for its narrower band gap of 3.0 eV [18]. The shapes of curves for mechanical milled TiO_2 showed no difference, because the phase composition was totally anatase after being annealed at 500°C.

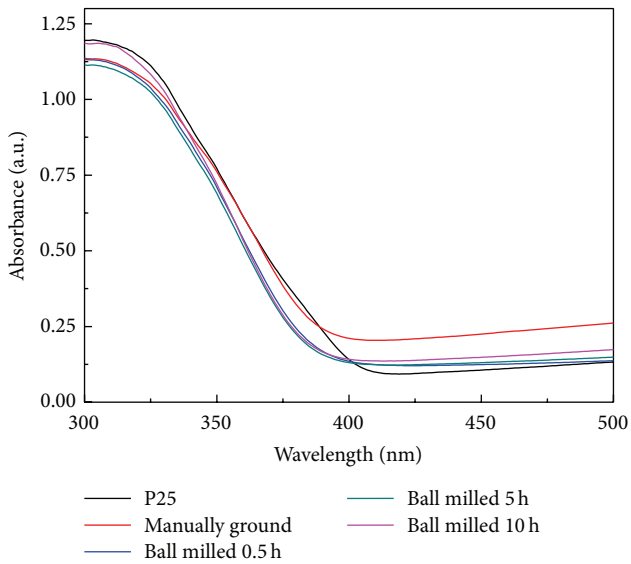

Figure 4: UV-visible absorption spectra of different TiO_2 films.

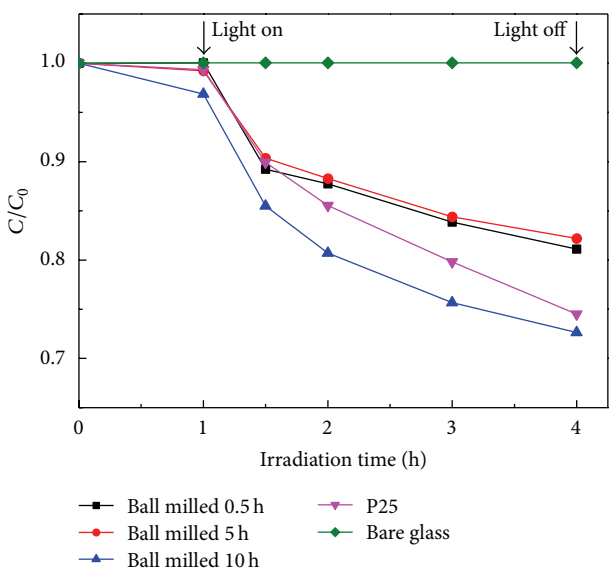

Figure 5: Photocatalytic degradation of methyl orange by different TiO_2 films.

3.5. Photocatalytic Activities of TiO_2 Films. Photocatalytic degradation activities of methyl orange by hierarchical TiO_2 and P25 films are shown in Figure 5. The results of degradation are reported as ratio of (C/C_0) versus illumination time (t). The initial concentration of MO solution was indicated by the initial absorbance and denoted by C_0, and the concentration of MO during reaction was denoted by C. For the selected milling time, a gradual increase in photocatalytic activity is observed with increasing ball milling time. The photocatalytic activity reached a maximum after 10 h of milling. Because of the larger surface area and high surface energy introduced by ball milling, 10 h milled TiO_2 could absorb more methyl orange. Besides, residual stress and lattice distortion may result in a good separation of electrons and holes to reduce the recombination rate [15, 16, 19, 20]. As a result, a larger amount of electrons and holes were available for the photocatalytic reaction. Therefore, a faster methyl orange degradation rate of 10 h milled film was observed. P25 shows a relatively faster degradation rate than the other samples, which may be due to the higher light absorbency.

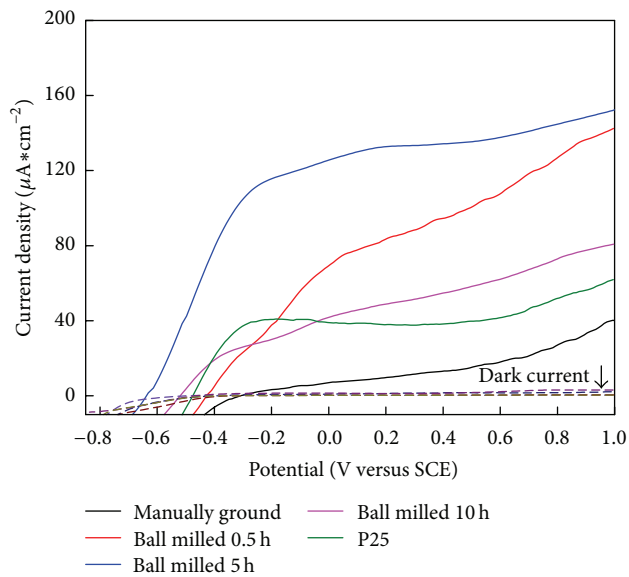

Figure 6: Photocurrent density versus applied potential curves of the films under UV illumination or in dark.

3.6. Photocurrent of TiO_2 Films. Photoelectrochemical properties of the photoanodes were characterized by linear sweep voltammetry. There were no obvious photocurrent responses for each photoanode in the dark, when the applied potential was linearly raised from −0.8 to 1 V (Figure 6). However, under UV illumination, photocurrents were distinctly detected for all the thin-film electrodes, showing a positive correlation to the applied potential which could reduce the recombination of photogenerated charge carriers. The relatively small surface area of disordered TiO_2 nanotubes limited the contact with electrolyte leading to the fact that the film obtained by manual grinding exhibited extremely poor performance in this measurement. However, the linear-like curve showed good charge transferring and collecting abilities of nanotubes. The 5 h milled film outperformed the other films in the photocurrent spectroscopy under UV irradiation in the whole applied potential range. The larger photocurrent densities of the hierarchical structured TiO_2 films are due to the coexistence of nanoparticles and nanotubes. Nanoparticles could increase surface area and nanotubes could act as light harvester and good charge carrier transporter and collector [12]. However, when milling time extended to 10 h, without nanotubes establishing an efficient charge carrier transfer pathway among the particles, the long zigzag transfer path introduces more recombination which leads to a relatively low photocurrent density. The varied open circuit potential may be due to the different morphology of the

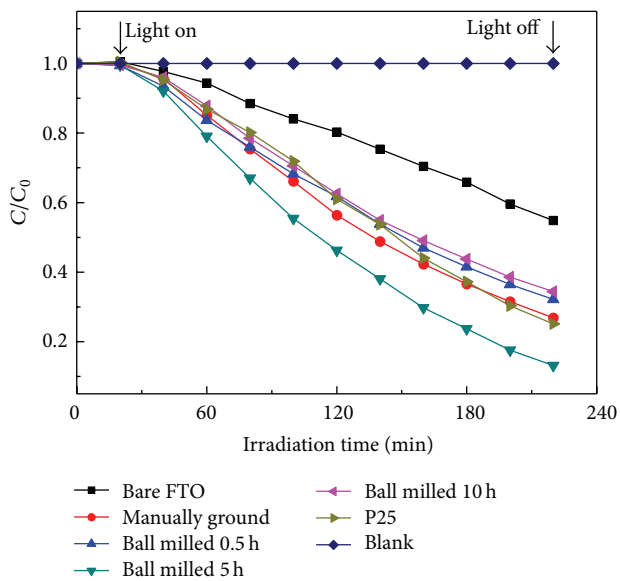

FIGURE 7: Photoelectrochemical catalytic activities of different TiO_2 films.

samples [21]. Interestingly, although P25 and the manually ground sample could absorb more light (even P25 has a large specific surface area of 57.4 m^2/g [22]), the photo currents (black and green lines) are much smaller than those of the hierarchical structured nanotubes (blue and red lines), which indicates that the nanotubes embedded in nanoparticles could collect more charge carriers and provide a direct pathway to FTO substrate.

3.7. Photoelectrochemical Catalytic Activities of the Films. As shown in Figure 7, photoelectrochemical catalytic activity of 5 h milled TiO_2 film is superior to those of the other films. The enhanced activity derived from the special hierarchical structure includes three aspects. Firstly, the fragments adhering to nanotubes could enlarge the surface area. Consequently, the films with hierarchical structure could provide more active sites for photocatalytic reaction [23]. Secondly, nanotubes could enhance light-harvesting and charge-separating abilities of films. Due to the existence of nanotubes, more light is scattered and multiply absorbed, which leads to the improvement of light-harvesting ability of the films and good absorption of UV light [24]. Thus, hierarchical structured TiO_2 nanotubes could harvest more light and generate more free charge carriers to induce photocatalysis under UV irradiation. Lastly, nanotubes could act as charge collectors, which could gather electrons from nanoparticles and provide the carriers with efficient paths [12]. The additional DC power supply drives the electrons transferring more easily, which means that more electrons are available for the photocatalytic reaction. Due to the high surface energy introduced by ball milling process, hierarchical TiO_2 nanotubes could absorb more reaction substrate, which results in a faster degradation in the initial tens of minutes. The degradation rate of P25 went faster in the last several minutes because of the influence of the anatase-rutile mixed phase. Due to the higher light

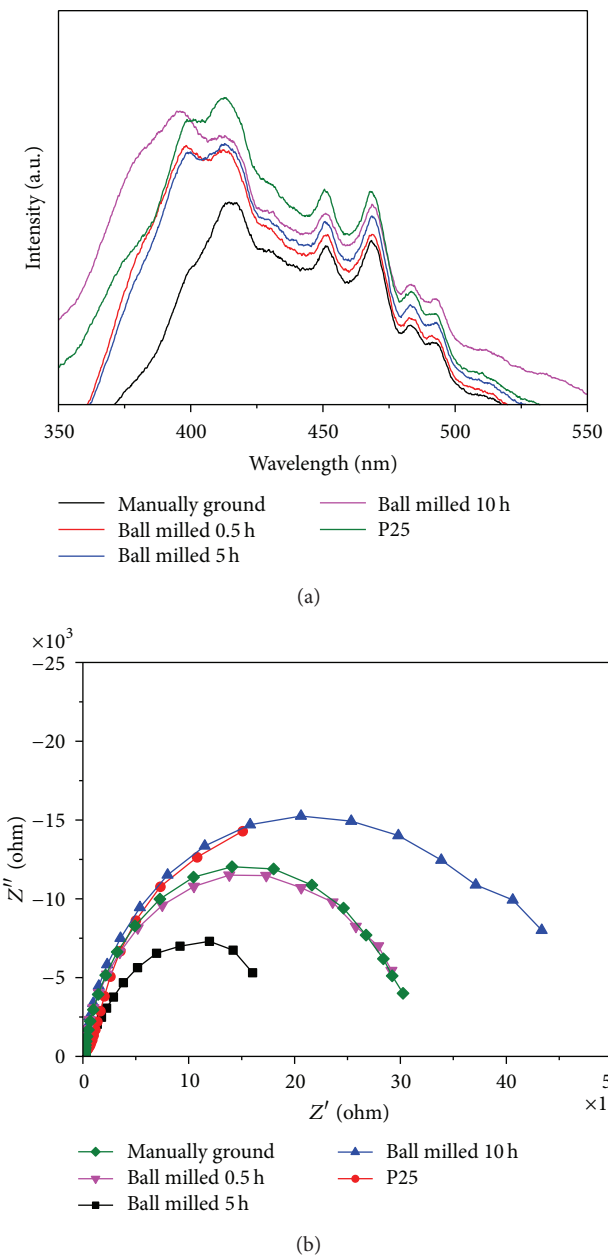

FIGURE 8: Photoluminescence spectra (a) and electrochemical impedance spectra (b) of TiO_2 films.

scattering ability, manually ground sample showed a slightly faster degradation rate, but it was still much lower than that of 5 h milled sample.

3.8. Photoluminescence Spectra and Electrochemical Impedance Spectra of the Films. To further discuss the separation of electrons and holes in hierarchical structured TiO_2 samples, photoluminescence (PL) spectra of the prepared films were investigated. As shown in Figure 8(a), a good separation of electrons and holes is observed in the pristine nanotubes. PL intensities increased with the extended milling time. This is due to the introduction of recombination centers through

milling process [25]. There is a strong peak at 398 nm, which is considered to be the emission of band gap transition as the energy of light is approximately equal to the band gap energy of anatase (387.5 nm). Four small peaks at the wavelengths of 451 nm, 468 nm, 483 nm, and 493 nm mainly resulted from surface oxygen vacancies and defects of the samples [26]. However, the intensities of all the prepared samples are lower than that of P25. As P25 contains 13.75% rutile phase, a strong peak is observed at 413 nm, which is equal to the band gap energy of rutile.

Then we also investigated electrochemical impedance spectra (EIS) of the prepared films. As shown in Figure 8(b), the semicircle at low frequency becomes much smaller after 5 h of ball milling, indicating a lower resistance of the electron transfer at TiO_2/electrolyte interface. As mentioned above, nanotubes in the hierarchical structure could reduce charge recombination and facilitate electron transfer due to their one-dimensional structure [27]. Because of the straight path provided by nanotubes, charge recombination rate could decrease and charge transfer rate increases. It is considered that the relatively larger size of the present nanotubes could enlarge the pore size to improve the diffusion of electrolyte, which is beneficial for electron transfer in electrolyte. Therefore, an enhanced photocatalytic activity was absorbed, as indicated in Figure 7.

4. Conclusions

Nanotube-based hierarchical structured TiO_2 was facilely prepared by a two-step method: highly ordered TiO_2 nanotube arrays were first fabricated through the anodization process and then followed by mechanical milling. The morphologies of 5 h milled hierarchical TiO_2 nanotubes exhibit a uniform corn-like shape. Furthermore, 5 h milled TiO_2 nanotubes exhibited preferable photoelectrochemical activity in comparison to P25. The superior catalytic activity is suggested to be due to the combined advantages of high surface area of nanoparticles, as well as rapid electron transfer and collection of the nanotubes in the hierarchical structure. It is believed that, through further optimization of the milling process, more uniform desirable porous nanotube with bonded nanoparticles can be achieved. The hierarchical structured TiO_2 nanotubes synthesized by this two-step method indicate not only an easy way to in situ modify/dope TiO_2 in the milling process but also flexible applications on solar cells and other photoelectrochemical devices.

Conflict of Interests

The authors declare that there is no conflict of interests regarding the publication of this paper.

Acknowledgments

This work was supported by National Nature Science Foundation of China (51202050, 51162007, and 51462008), Hainan Provincial Program for International S&T Cooperation (KJHZ2013-13), and the Key S&T Project of Hainan Province (ZDXM2014097).

References

[1] L. Jing, J. Zhou, J. R. Durrant, J. Tang, D. Liu, and H. Fu, "Dynamics of photogenerated charges in the phosphate modified TiO_2 and the enhanced activity for photoelectrochemical water splitting," *Energy and Environmental Science*, vol. 5, no. 4, pp. 6552–6558, 2012.

[2] W. Zheng, X. Li, G. He, X. Yan, R. Zhao, and C. Dong, "A highly responsive UV photodetector based on hierarchical TiO_2 nanorod/nanoparticle composite," *RSC Advances*, vol. 4, no. 41, pp. 21340–21346, 2014.

[3] A. Fujishima and K. Honda, "Electrochemical photolysis of water at a semiconductor electrode," *Nature*, vol. 238, no. 5358, pp. 37–38, 1972.

[4] S. Lin, D. Li, J. Wu, X. Li, and S. A. Akbar, "A selective room temperature formaldehyde gas sensor using TiO_2 nanotube arrays," *Sensors and Actuators B: Chemical*, vol. 156, no. 2, pp. 505–509, 2011.

[5] D. Li, N. Pan, J. Liao, X. Cao, and S. Lin, "Effects of surface modification of TiO_2 nanotube arrays on the performance of cds quantum-dot-sensitized solar cells," *International Journal of Photoenergy*, vol. 2013, Article ID 129621, 10 pages, 2013.

[6] J. Liao, S. Lin, L. Zhang, N. Pan, X. Cao, and J. Li, "Photocatalytic degradation of methyl orange using a TiO_2/Ti mesh electrode with 3D nanotube arrays," *ACS Applied Materials & Interfaces*, vol. 4, no. 1, pp. 171–177, 2012.

[7] J. H. Park, S. Kim, and A. J. Bard, "Novel carbon-doped TiO_2 nanotube arrays with high aspect ratios for efficient solar water splitting," *Nano Letters*, vol. 6, no. 1, pp. 24–28, 2006.

[8] D. R. Baker and P. V. Kamat, "Disassembly, reassembly, and photoelectrochemistry of etched TiO_2 nanotubes," *Journal of Physical Chemistry C*, vol. 113, no. 41, pp. 17967–17972, 2009.

[9] C. A. Grimes, "Synthesis and application of highly ordered arrays of TiO_2 nanotubes," *Journal of Materials Chemistry*, vol. 17, no. 15, pp. 1451–1457, 2007.

[10] K. Shankar, J. Bandara, M. Paulose et al., "Highly efficient solar cells using TiO_2 nanotube arrays sensitized with a donor-antenna dye," *Nano Letters*, vol. 8, no. 6, pp. 1654–1659, 2008.

[11] X. Zhang, J. Zhou, Y. Gu, and D. Fan, "Visible-light photocatalytic activity of N-doped TiO_2 nanotube arrays on acephate degradation," *Journal of Nanomaterials*, vol. 2015, Article ID 527070, 6 pages, 2015.

[12] Y. Bai, H. Yu, Z. Li, R. Amal, G. Q. Lu, and L. Wang, "In situ growth of a ZnO nanowire network within a TiO_2 nanoparticle film for enhanced dye-sensitized solar cell performance," *Advanced Materials*, vol. 24, no. 43, pp. 5850–5856, 2012.

[13] B. Tan and Y. Wu, "Dye-sensitized solar cells based on anatase TiO_2 nanoparticle/nanowire composites," *The Journal of Physical Chemistry B*, vol. 110, no. 32, pp. 15932–15938, 2006.

[14] G. Wu, J. Zhang, X. Wang et al., "Hierarchical structured TiO_2 nano-tubes for formaldehyde sensing," *Ceramics International*, vol. 38, no. 8, pp. 6341–6347, 2012.

[15] X. Pan and X. Ma, "Phase transformations in nanocrystalline TiO_2 milled in different milling atmospheres," *Journal of Solid State Chemistry*, vol. 177, no. 11, pp. 4098–4103, 2004.

[16] P. Xiaoyan, C. Yi, M. Xueming, and Z. Lihui, "Phase transformation of nanocrystalline anatase powders induced by mechanical activation," *Journal of the American Ceramic Society*, vol. 87, no. 6, pp. 1164–1166, 2004.

[17] G. B. Song, J. K. Liang, F. S. Liu, T. J. Peng, and G. H. Rao, "Preparation and phase transformation of anatase–rutile crystals in metal doped TiO_2/muscovite nanocomposites," *Thin Solid Films*, vol. 491, no. 1-2, pp. 110–116, 2005.

[18] A. Amtout and R. Leonelli, "Optical properties of rutile near its fundamental band gap," *Physical Review B*, vol. 51, no. 11, pp. 6842–6851, 1995.

[19] Y.-J. Lee, T.-G. Kim, and Y.-M. Sung, "Lattice distortion and luminescence of CdSe/ZnSe nanocrystals," *Nanotechnology*, vol. 17, no. 14, article no. 030, pp. 3539–3542, 2006.

[20] D. C. Hurum, K. A. Gray, T. Rajh, and M. C. Thurnauer, "Recombination pathways in the degussa P25 formulation of TiO_2: surface versus lattice mechanisms," *The Journal of Physical Chemistry B*, vol. 109, no. 2, pp. 977–980, 2005.

[21] M. D. Perez, C. Borek, S. R. Forrest, and M. E. Thompson, "Molecular and morphological influences on the open circuit voltages of organic photovoltaic devices," *Journal of the American Chemical Society*, vol. 131, no. 26, pp. 9281–9286, 2009.

[22] K. Suttiponparnit, J. Jiang, M. Sahu, S. Suvachittanont, T. Charinpanitkul, and P. Biswas, "Role of surface area, primary particle size, and crystal phase on titanium dioxide nanoparticle dispersion properties," *Nanoscale Research Letters*, vol. 6, no. 1, pp. 1–8, 2011.

[23] A. M. Doyle, S. K. Shaikhutdinov, S. D. Jackson, and H.-J. Freund, "Hydrogenation on metal surfaces: why are nanoparticles more active than single crystals?" *Angewandte Chemie*, vol. 42, no. 42, pp. 5240–5243, 2003.

[24] K. Zhu, N. R. Neale, A. Miedaner, and A. J. Frank, "Enhanced charge-collection efficiencies and light scattering in dye-sensitized solar cells using oriented TiO_2 nanotubes arrays," *Nano Letters*, vol. 7, no. 1, pp. 69–74, 2007.

[25] Q. Xiang, K. Lv, and J. Yu, "Pivotal role of fluorine in enhanced photocatalytic activity of anatase TiO_2 nanosheets with dominant (001) facets for the photocatalytic degradation of acetone in air," *Applied Catalysis B: Environmental*, vol. 96, no. 3-4, pp. 557–564, 2010.

[26] J. C. Yu, W. Ho, Z. Jiang, and L. Zhang, "Effects of F- doping on the photocatalytic activity and microstructures of nanocrystalline TiO_2 powders," *Chemistry of Materials*, vol. 14, no. 9, pp. 3808–3816, 2002.

[27] K. Fan, W. Zhang, T. Peng, J. Chen, and F. Yang, "Application of TiO_2 fusiform nanorods for dye-sensitized solar cells with significantly improved efficiency," *The Journal of Physical Chemistry C*, vol. 115, no. 34, pp. 17213–17219, 2011.